Supporting Information

Dual Vacancy-Regulated Pathway of Photoreduction of CO_2 on $Bi_{19}S_{27}Cl_3$ Nanorods into Multi-Carbon Solar Fuels

Tingting Cheng,[1#] Wangqiang Lin,[2#] Guangyu Chen,[3] Yong Yang,[4] Yongcai Zhang,[5] Junnan Qu,[6] Yichen Feng,[1] Qiang Li,[2*] Ran Long,[3] Jinlan Wang,[2] Yujie Xiong,[3] Yong Zhou,[1,7*] Zhigang Zou[1,7]

[1]Key Laboratory of Modern Acoustics (MOE), Institute of Acoustics, School of Physics, National Laboratory of Solid State Microstructures, Collaborative Innovation Center of Advanced Microstructures, Eco-Materials and Renewable Energy Research Center (ERERC), Jiangsu Key Laboratory for Nano Technology, Nanjing University, Nanjing, Jiangsu 210093, P. R. China.

[2]School of Physics, Southeast University, Nanjing, Jiangsu, 211189, P. R. China.

[3]National Synchrotron Radiation Laboratory, University of Science and Technology of China, Hefei, Anhui, 230026, P. R. China.

[4]School of Chemistry and Chemical Engineering, Nanjing University of Science and Technology, Nanjing, Jiangsu, 210094, P. R. China.

[5]School of Chemistry and Chemical Engineering, Yangzhou University, Yangzhou 225009, P. R. China. [6]Jiangsu Key Laboratory of Advanced Metallic Materials, School of Materials Science and Engineering, Southeast University, Nanjing 211189, China.

[6]Jiangsu Key Laboratory of Advanced Metallic Materials, School of Materials Science and Engineering, Southeast University, Nanjing, Jiangsu, 211189, China.

[7]School of Science and Engineering, The Chinese University of Hongkong (Shenzhen), Shenzhen, Guangdong 518172, P. R. China.

1. Experimental

1.1 Preparation

BSC nanowires were synthesized by a hydrothermal route.[1] The raw materials including Bismuth (III) chloride ($BiCl_3$), thiourea (CH_4N_2S,) and ethylene diamine tetraacetic acid (EDTA) were used without further purification. In a typical process, 2.5 mmol $BiCl_3$, 2.3 mmol CH_4N_2S and 0.5 mmol EDTA were mixed into 30 ml ethanol, after magnetic vigorous stirring for 1 h to ensure the complete dissolution of the reagents. Then the solution was subjected to reaction at 180 °C for 72 h in a 50 mL Teflon-lined autoclave. The product precipitated in the autoclave was washed several times using deionized water and absolute ethanol to remove impurity ions, followed by 3 days of freeze-dried as BSC product.

Amount of as-prepared BSC powder dispersed into a porcelain boat, then transferred to a muffle furnace and then heated to 300 °C at a heating rate of 5 °C min^{-1} in Ar_2 (5% H_2) and kept for 1 h. The samples were removed out after naturally cooled to room temperature and named Vs-BSC.

0.1g as-prepared BSC powder was spread flat on a crucible plate and operated in Ar_2 (containing 5% H_2) plasma chamber. Prior to the commencement of processing, Ar_2 (containing 5% H_2) was introduced and pumped into the quartz tube reactor for 20 min to remove any residual air. In the plasma exposure step, the applied pressure was 150 Pa and argon plasma was produced by radio frequency (RF) discharge (100 W, 13.56 MHz). The treatment time is carefully controlled to 30 s, then the samples were quickly collected and stored under vacuum preservation as V_{Bi+S}-BSC.

1.2 Characterization

The crystal structure of samples were examined by X-ray diffractometer (XRD, Rigaku Ultima III, Japan) using Cu-Kα radiation (λ = 0.15406 nm) at 40 kV and 40mA with a scan rate of 5° min^{-1}. The morphology was characterized on scanning electron microscope (SEM, Zeiss Gemini 500) and transmission electron microscope (TEM, FEI Tecnai F20 G2 F20S-TWIN). The states of

the elements were acquired from X-ray photoelectron spectrometer (XPS, ULVAC-PHI PHI5000 VersaProbe) and standardizing according to the binding energy of the adventitious C 1s peak at 284.8 eV, which was used to inspect the chemical states. The CO_2 adsorption isotherms of the materials were measured at 273.15 K in the relative pressure range of 0.001-0.03 on the porosity analyzer (TriStar 3000, Micromeritics, USA). Ultraviolet-visible diffuse reflection spectra were investigated by a UV-vis spectrophotometer (UV-vis DRS, Shimadzu UV-2550). Electron paramagnetic resonance (EPR) spectra were performed using Bruker Magnettech ESR5000. The detection of ^{13}C isotope in $^{13}C_2H_6$ was detected by mass spectrometry (QP2010SE, Shimadzu, Japan). In situ DRIFTS was recorded with Bruker IFS 66v Fourier-transform spectrometer equipped with a Harrick diffuse reflectance accessory at the Infrared Spectroscopy and Microspectroscopy Endstation (BL01B) of NSRL in Hefei. The X-ray absorption fine structure spectra (XAFS) at the Bi K-edge of the materials were operated at the BL14W Beam line station in the Shanghai Synchrotron Radiation Facility (SSRF). The spectra were processed and analyzed by the software codes Athena. The electrochemical impedance spectroscopy (EIS) and photocurrent response measurements were conducted on CHI660E electrochemical workstation using 1 mM $NaSO_4$ solution as electrolyte.

1.3 Photocatalytic testing

The reaction of photocatalytic CO_2 reduction were performed in a Pyrex reaction vessel with a volume of 460 mL equipped with circulating water at room temperature. A 300 W xenon arc lamp (PLS-SXE300+, Perfectlight, China) was used as sunlight simulator source. Typically, 20 mg samples were uniformly dispersed on the quartz wool with an area of 4.2 cm^2, then 0.3 ml deionized water was poured into stainless steel reactor. Before irradiating, the reactor vessel was filled with high purity CO_2 to 1 atm. During the reaction, 0.5mL of gas was taken from the reaction headspace every hour and analyzed by gas chromatography (Agilent 8890, USA).

The electron-based selectivity of C_2H_6 was calculated using (1):

$$Sel_{electron}(C_2H_6)\left(\frac{n(C_2H_6)\times 14}{n(CO)\times 2+n(CH_4)\times 8+n(C_2H_6)\times 14}\right)\times 100\% \quad (1)$$

where n is the formation rate.

1.4 Computational Details

All density functional theory (DFT) calculations are performed with the Vienna ab initio simulation package (VASP).[2] The ion-electron interaction is described by the projector-augmented wave method. The exchange-correlation potentials are treated within the generalized gradient approximation in the form of the Perdew-Burke-Ernzerhof (PBE) functional.[3-5] Moreover, spin polarizations are taken into consideration in this work. A plane-wave cutoff energy of 500 eV for the plain wave basis set is used.

The bulk structure of intrinsic BSC ($Bi_{114}S_{162}Cl_{18}$), with the lattice parameters of a = b = 27.12 Å, c = 12.27 Å and α = β = 90°, γ = 120°, is relaxed using a conjugate gradient method until the energies and each component of the forces converged to 10^{-5} eV and 0.001 eV $Å^{-1}$. The Brillouin zone is sampled using a Monkhorst-Pack mesh with a 1 × 1 × 3 k-point grid in reciprocal space. Based on the optimized bulk structure above, BSC (220) surface ($Bi_{57}S_{81}Cl_9$) is built with 3 layers thickness (1 layer thickness is 2.96 Å), where the bottom one layer is fixed to simulate the bulk structure, while the top two layers are relaxed to simulate the surface structure, and 15 Å vacuum is added to avoid interactions among periodic images. The surface structures, including intrinsic BSC(220) surface and vacancy defect, as well as the structure of subsequent adsorbed intermediates, are optimized with the van der Waals interactions are calculated by using the empirical correction in of Grimme's scheme (DFT-D3),[6,7] and the convergence criteria for the force and total energy component during structure optimizations are carried out by employing the conjugated gradient method with convergence thresholds of 0.02 eV/Å and 1.0×10^{-5} eV, respectively, and the Brillouin zone-sampling is restricted to the gamma point in the structure optimizations. For the calculation

of electronic structure, including Bader analysis, density of states (DOS) and electron density difference diagram, based on the above optimized structures, the Brillouin zone is sampled using a Monkhorst-Pack mesh with a 3 × 2 × 1 k-point grid in reciprocal space. And the Gibbs free energy change (ΔG) for each elementary reaction is calculated as $\Delta G = \Delta E + \Delta E_{ZPE} - T\Delta S$, where ΔE represents the electronic energy difference obtained from products and reactants, ΔE_{ZPE} and ΔS represent the changes of the zero-point energies (ZPE) and entropy (S), respectively, which are obtained from the vibrational frequency calculations through the VASPKIT code.[8]

2. Supplementary data

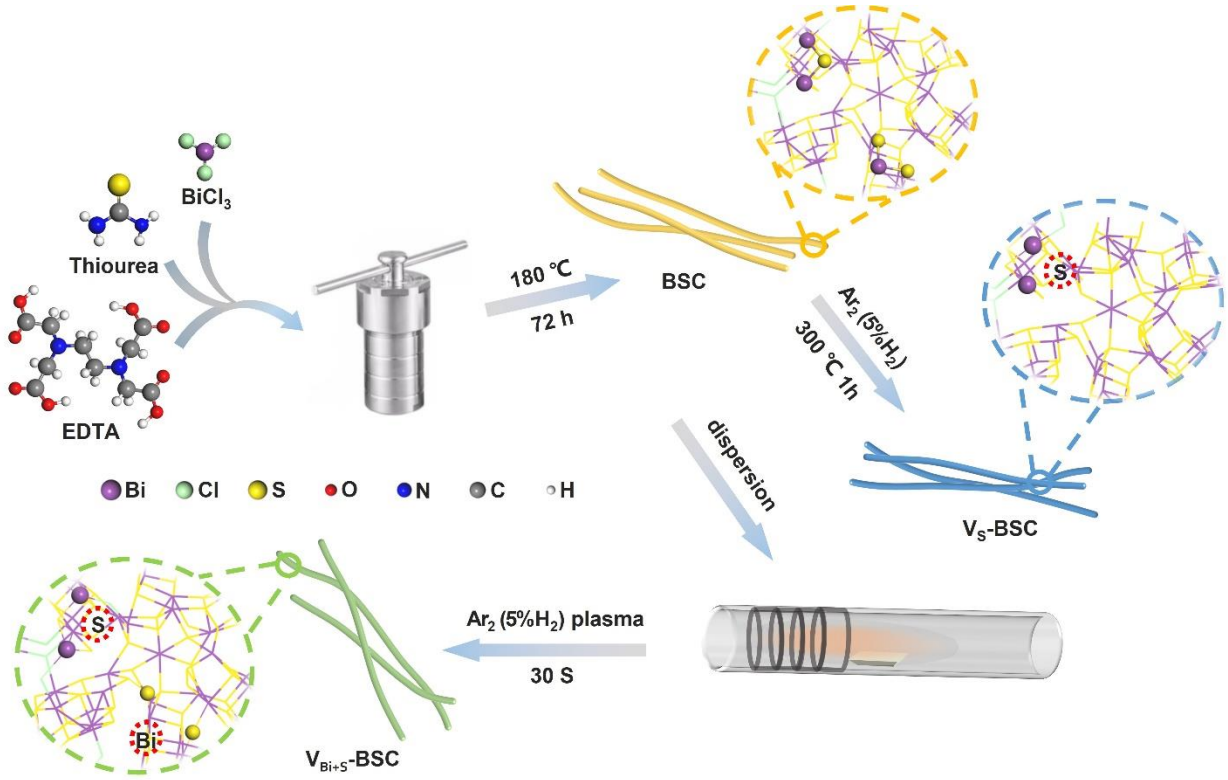

Figure S1. Schematic depiction of the preparation process for BSC nanowires and V_{Bi+S}-BSC.

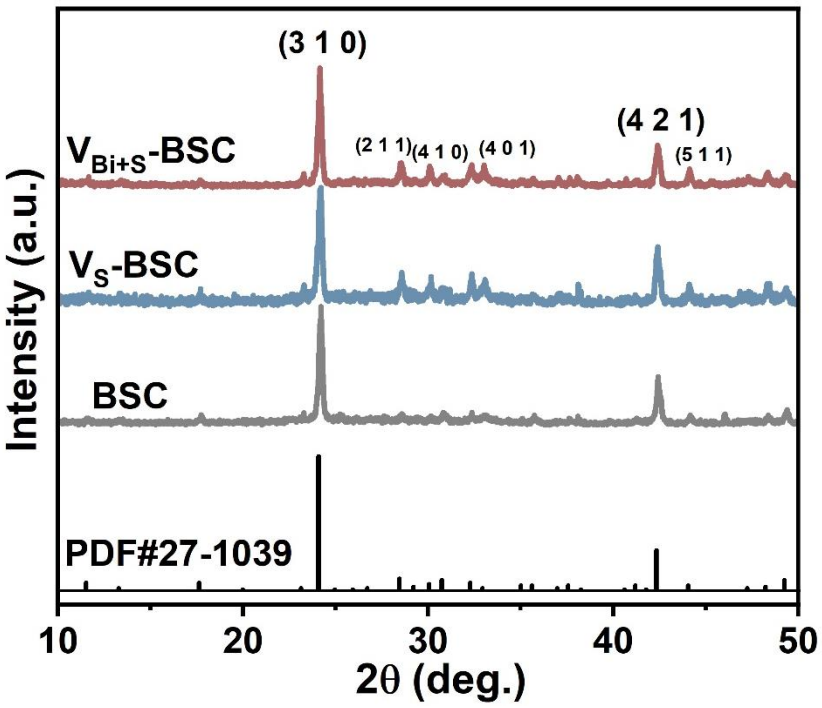

Figure S2. XRD patterns of BSC, V_S-BSC and V_{Bi+S}-BSC.

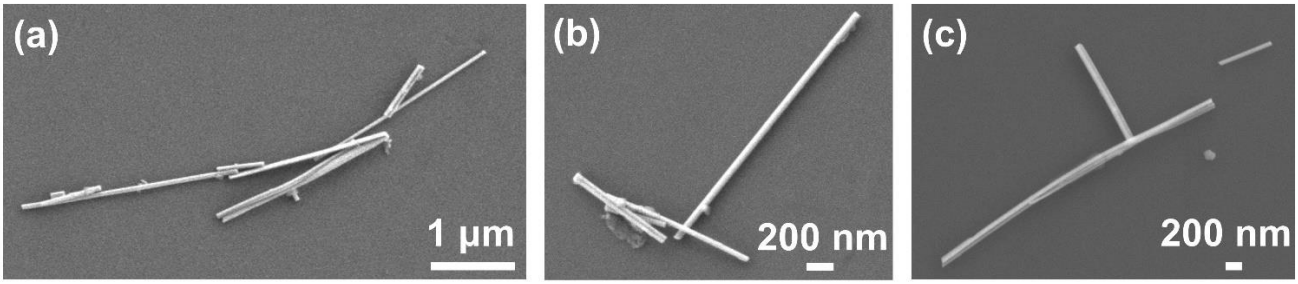

Figure S3. SEM images of (a) BSC, (b) V_S-BSC and (c) V_{Bi+S}-BSC.

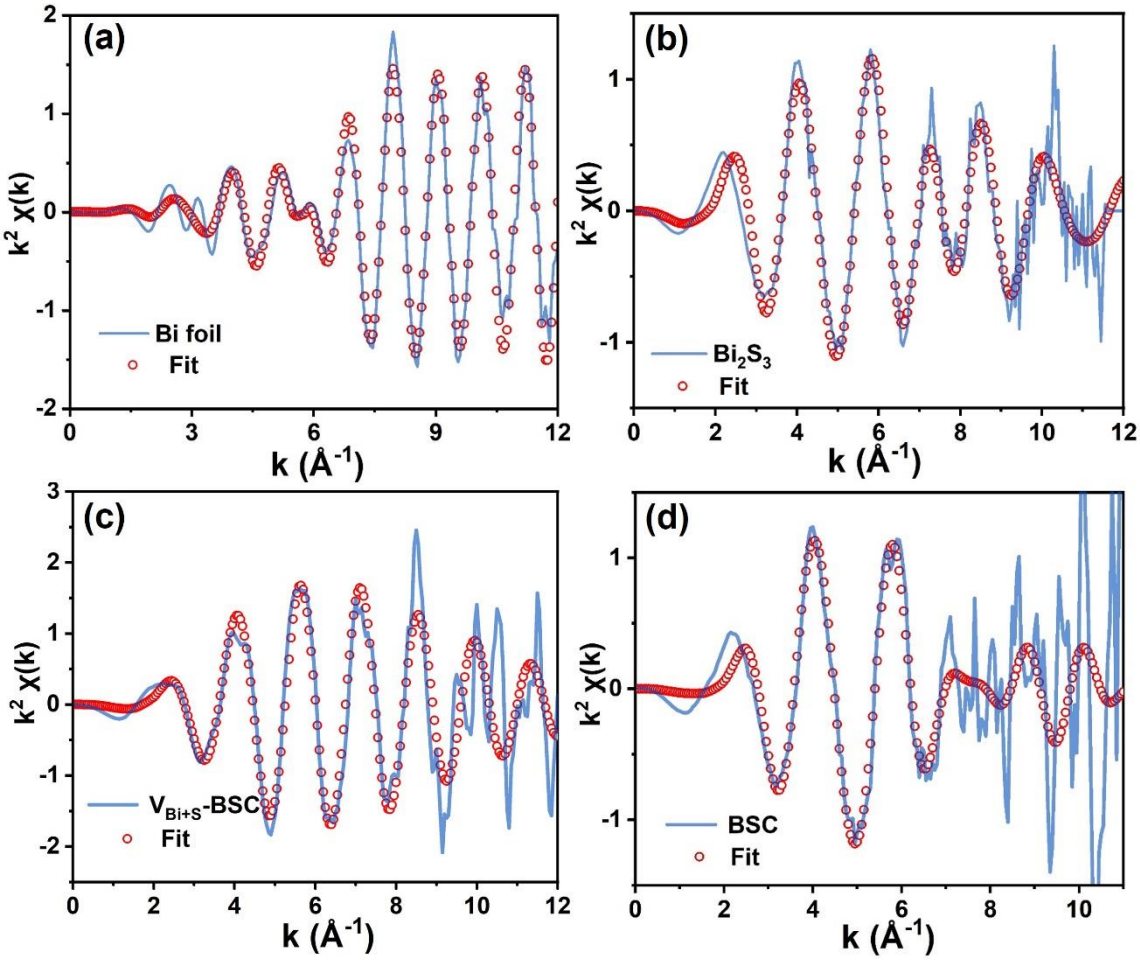

Figure S4. Bi L_3- edge EXAFS spectra and fit curve for Bi foil, Bi_2S_3, BSC and V_{Bi+S}-BSC in the k-space.

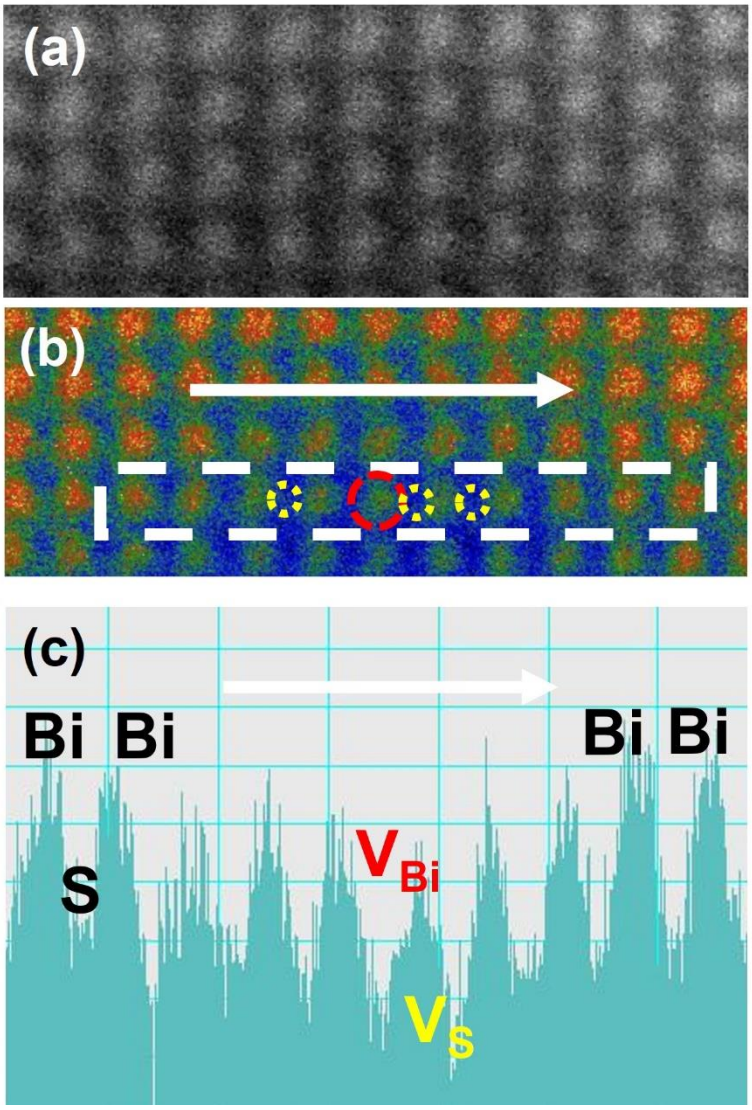

Figure S5. (a) STEM images and (b) temperature-colored STEM images schematic illustration of V_{Bi+S}-BSC crystal structure. (c) The intensity profile corresponding to the white square in (b).

Table S1. EXAFS fitting parameters at the Bi L_3-edge for various samples.

Sample	Path	Coordination number	R (Å)	σ^2
Bi-foil	Bi-Bi	3.0	3.06	0.0051
	Bi-Bi	3.0	3.55	0.0199
Bi_2S_3	Bi-S	3.0	2.11	0.0079
BSC	Bi-S	0.1	1.45	0.0023
	Bi-S	3.9	2.08	0.0202
	Bi-Cl	1.4	2.99	0.0160
V_{Bi+S}-BSC	Bi-S	0.1	1.43	0.0085
	Bi-S	2.9	2.02	0.0195
	Bi-Cl	1.2	3.03	0.0123

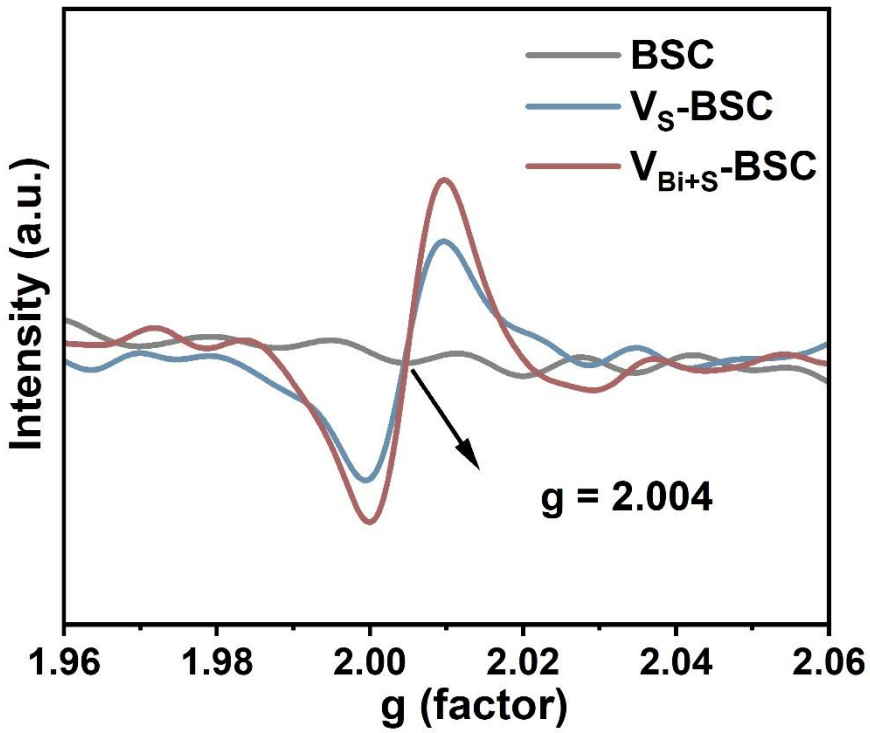

Figure S6. EPR spectra of BSC, V_S-BSC and V_{Bi+S}-BSC.

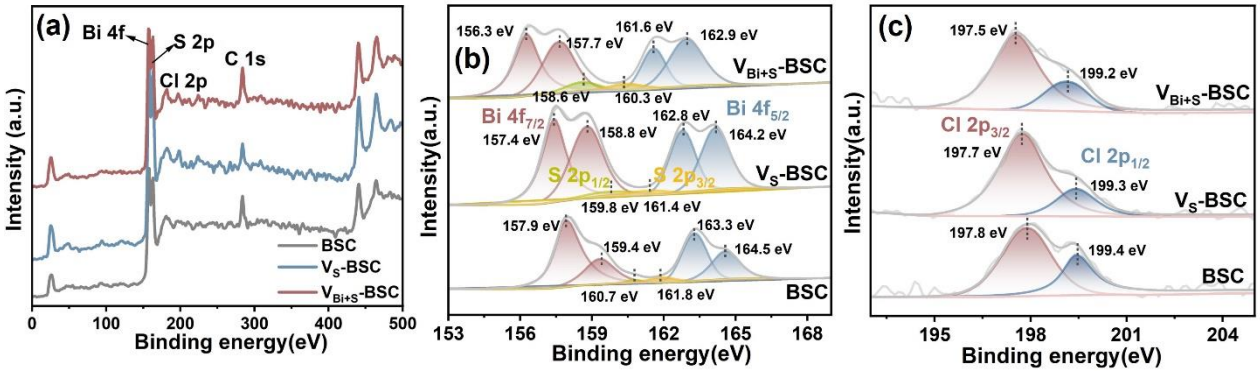

Figure S7. (a) Full scan XPS spectrum, (b) Bi 4f and (c) Cl 2p XPS spectra of BSC, V_S-BSC and V_{Bi+S}-BSC.

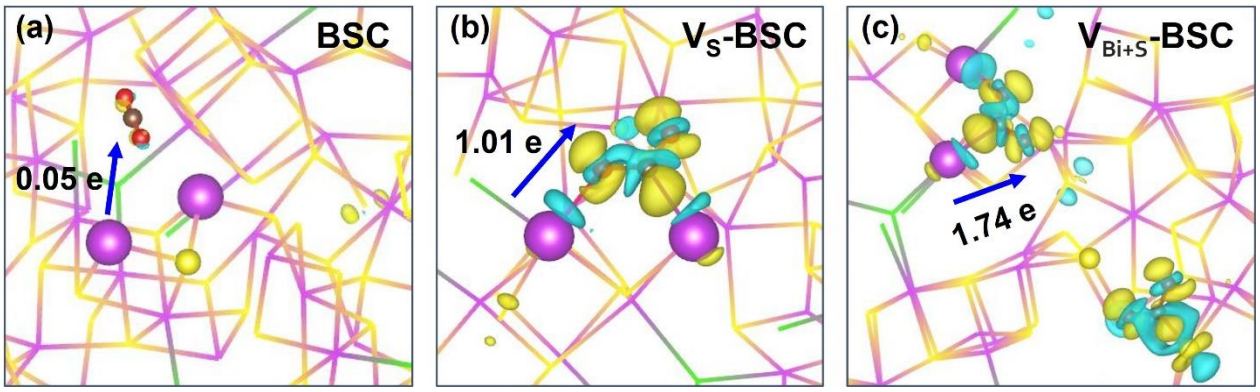

Figure S8. Side view of the charge density difference for *CO_2 adsorbed on (a) BSC with the iso-value of 0.001 a.u., (b) V_S-BSC and (c) V_{Bi+S}-BSC with the iso-value of 0.005 a.u., Charge depletion and accumulation are presented in cyan and yellow, respectively.

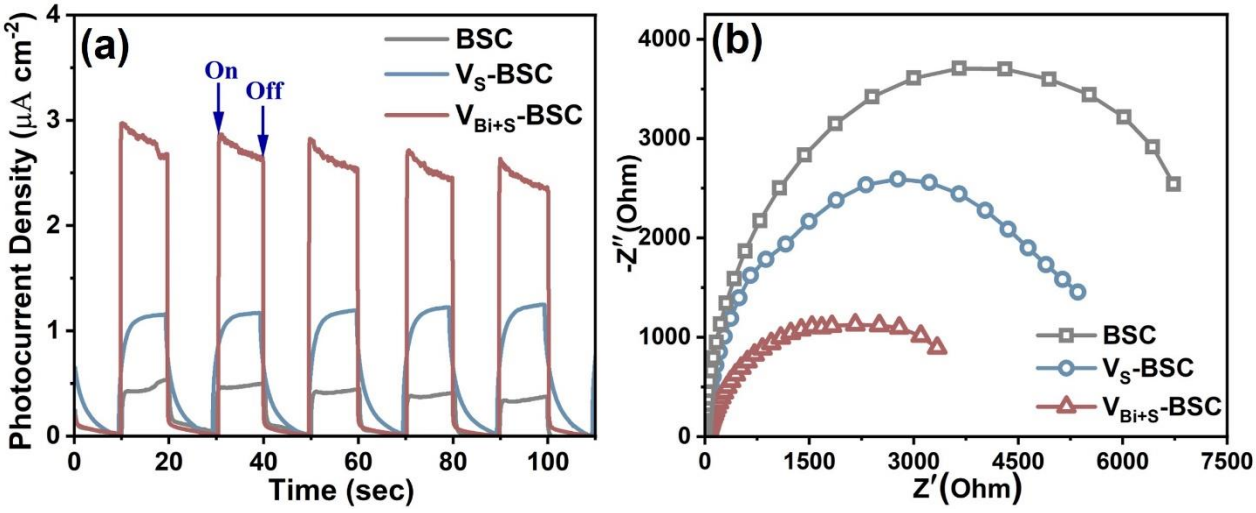

Figure S9. (a) Photocurrent response spectra and (b) EIS spectra of BSC, V_S-BSC and V_{Bi+S}-BSC.

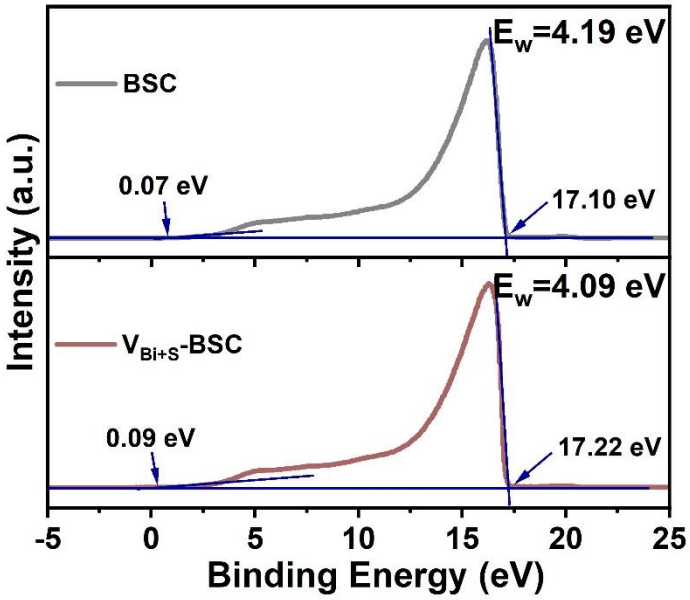

Figure S10. UPS spectra of BSC and V_{Bi+S}-BSC.

The work function of BSC and V_{Bi+S}-BSC is obtained by the formula $\Phi = h\nu-(E_{Fermi} - E_{Cutoff})$ ($h\nu$ is the photon energy, E_{Fermi} is the high kinetic energy starting edge, E_{Cutoff} is the low kinetic energy cutoff edge, $h\nu$ = 21.22 eV) .

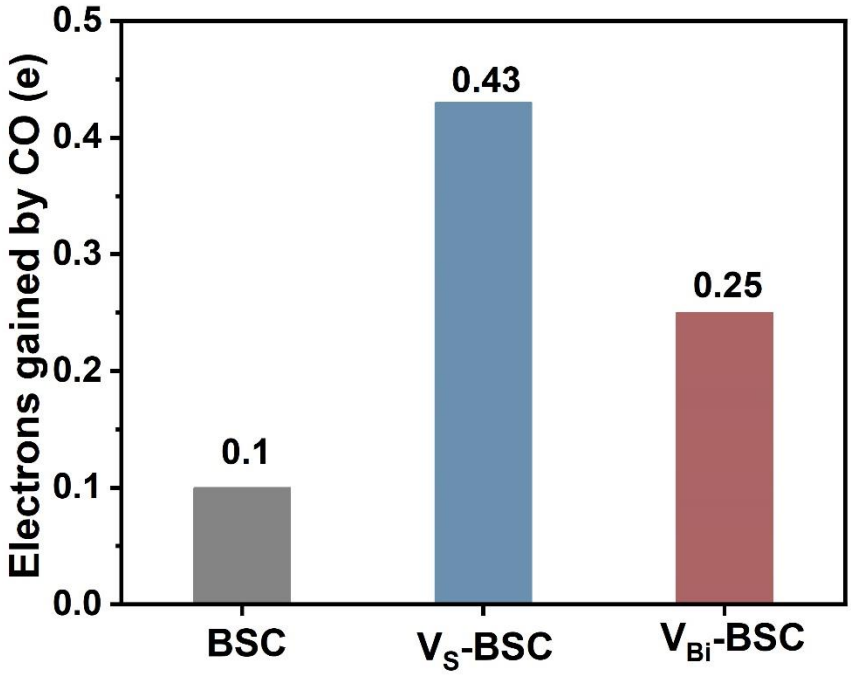

Figure S11. Electrons gained by adsorbed CO simulated by Bader analysis.

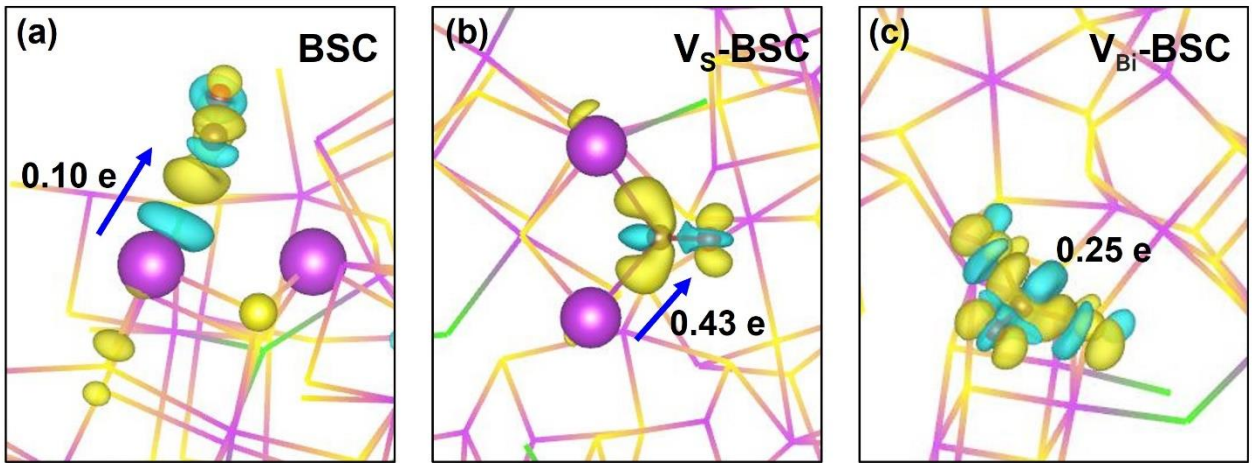

Figure S12. Side view of the charge density difference for *CO adsorbed on (a) BSC with the iso-value of 0.001 a.u., (b) V_S-BSC and (c) V_{Bi}-BSC with the iso-value of 0.005 a.u., Charge depletion and accumulation are presented in cyan and yellow, respectively.

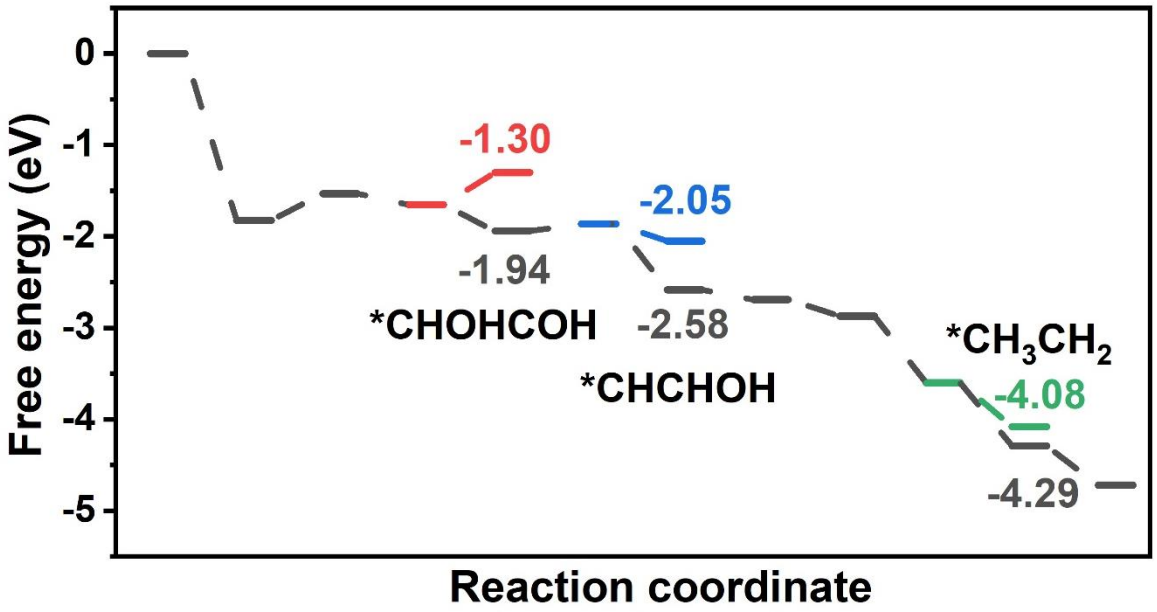

Figure S13. Gibbs free energy diagrams of CO_2 reduction to CH_3CH_3 on V_{Bi+S}-BSC units.

During the ydrogenation steps, three potential pathways are also considered. The first possibility involves hydrogenation of the *COHCOH intermediate, leading to two potential intermediates, namely *CHOHCOH and *COHCHOH (corresponding to the red and grey lines in the figure, respectively). Since the formation of the *CHOHCOH intermediate has a lower energy, the *COHCOH intermediate is more inclined to form *CHOHCOH. Similarly, for the second possibility, by comparing the blue and grey lines in the figure, the *CHOHCHOH intermediate prefers to form *CHCHOH. For the third possibility, by contrasting the green and grey lines, the *CH_2CH_2 intermediate is more likely to form *CH_3CH_2 rather than *CH_2CH_3.

$CO_2 + * \rightarrow *CO_2$ (1)

$*CO_2 + H^+ + e^- \rightarrow *COOH$ (2)

$*COOH + H^+ + e^- \rightarrow *CO + H_2O$ (3)

$*CO + *CO \rightarrow *OCCO$ or $*CO \rightarrow CO\uparrow + *$ (4)

$*OCCO + H^+ + e^- \rightarrow *OCCOH$ (5)

$*OCCOH + H^+ + e^- \rightarrow *COHCOH$ (6)

$*COHCOH + H^+ + e^- \rightarrow *CHOHCOH$ (7)

$*CHOHCOH + H^+ + e^- \rightarrow *CHOHCHOH$ (8)

$*CHOHCHOH + H^+ + e^- \rightarrow *CHCHOH + H_2O$ (9)

$*CHCHOH + H^+ + e^- \rightarrow *CH_2CHOH$ (10)

$*CH_2CHOH + H^+ + e^- \rightarrow *CH_2CH_2 + H_2O$ (11)

$*CH_2CH_2 + H^+ + e^- \rightarrow *CH_3CH_2$ (12)

$*CH_3CH_2 + H^+ + e^- \rightarrow CH_3CH_3\uparrow + *$ (13)

Figure S14. Proposed reaction process for the photothermal reduction of CO_2 to C_2H_6 of the V_{Bi+S}-BSC.

References

1. Z. Wu, Y. Jiang, X. Xiong, S. Ding, Y. Shi, X. Liu, Y. Liu, Z. Huang, J. Hu, *Catal. Sci. Technol.* **2017**, *7*, 3464-3468.

2. Kresse, G.; Furthmüller, J. Efficient iterative schemes for ab initio total-energy calculations using a plane-wave basis set. *Phys. Rev. B* **1996**, *54*, 11169-11186.

3. Blöchl, P. E. Projector augmented-wave method. *Phys. Rev. B* **1994**, *50*, 17953-17979.

4. Perdew, J. P.; Burke, K.; Ernzerhof, M. Generalized Gradient Approximation Made Simple. *Phys. Rev. Lett.* **1996**, *77*, 3865-3868.

5. Perdew, J. P.; Ernzerhof, M.; Burke, K. Rationale for mixing exact exchange with density functional approximations. *J. Chem. Phys.* **1996**, *105*, 9982-9985.

6. Grimme, S. Semiempirical GGA-type density functional constructed with a long-range dispersion correction. *J. Comput. Chem.* **2006**, *27*, 1787-1799.

7. Grimme, S.; Antony, J.; Ehrlich, S.; Krieg, H. A consistent and accurate ab initio parametrization of density functional dispersion correction (DFT-D) for the 94 elements H-Pu. *J. Chem. Phys.* **2010**, *132*, 154104.

8. Wang, V.; Xu, N.; Liu, J.-C.; Tang, G.; Geng, W.-T. VASPKIT: A user-friendly interface facilitating high-throughput computing and analysis using VASP code. *Comput. Phys. Commun.* **2021**, *267*, 108033.